Piezoelectric Polymeric Bicomponent Fibers Produced by Melt Spinning

Anja Lund,[1,2] Christian Jonasson,[3] Christer Johansson,[3] Daniel Haagensen,[2] Bengt Hagström[2,4]

[1]*The Swedish School of Textiles, University of Borås, SE-501 90 Borås, Sweden*
[2]*Department of Materials and Manufacturing Technology, Chalmers University of Technology, SE-412 96 Göteborg, Sweden*
[3]*The Imego Institute, Arvid Hedvalls Backe 4, SE-400 14 Göteborg, Sweden*
[4]*Textiles and Plastics Department, Swerea IVF, Box 104, SE-431 22 Mölndal, Sweden*

Received 22 June 2011; accepted 6 January 2012
DOI 10.1002/app.36760
Published online in Wiley Online Library (wileyonlinelibrary.com).

ABSTRACT: Melt spinning of a novel piezoelectric bicomponent fiber, with poly(vinylidene fluoride) as the electroactive sheath component, has been demonstrated. An electrically conductive compound of carbon black (CB) and high density polyethylene was used as core material, working as an inner electrode. A force sensor consisting of a number of fibers embedded in a soft CB/polyolefin elastomer matrix was manufactured for characterization. The fibers showed a clear piezoelectric effect, with a voltage output (peak-to-peak) of up to 40 mV under lateral compression. This continuous all-polymer piezoelectric fiber introduces new possibilities toward minimal single fiber sensors as well as large area sensors produced in standard industrial weaving machines. © 2012 Wiley Periodicals, Inc. J Appl Polym Sci 000: 000–000, 2012

Key words: fibers; carbon black; sensors

INTRODUCTION

Since the discovery of its strong piezoelectric effect in 1969,[1,2] poly(vinylidene fluoride) (PVDF) has been extensively researched. It is now commercially available as films or coaxial cables for a variety of transducer applications.[3] The piezoelectric effect in a material stems from a nonsymmetry in the atomic structure of its crystalline units, causing the crystallites to act as dipoles. PVDF is polymorphic, i.e., it can crystallize in at least four different phases known as α, β, γ, and δ. The α-phase, also known as Form II, has a monoclinic unit cell and the chains are of a TGTG′ conformation (T = trans; G = gauche). It is formed when PVDF is crystallized from the melt or in solution-cast films. This structure is nonpolar due to the cancellation of the dipoles exhibited by the two polar chains that make up the unit cell.[4–8] The β-phase, or Form I, has an orthorhombic unit cell, consisting of two chains in an all-trans (TTTT) conformation. The β-phase structure is polar and thus useful as a base for a piezoelectric material.[4–9] The conformation of the γ-phase is TTTGTTTG′. This phase is also polar and appears in PVDF crystallized at a high temperature and/or under a high pressure. It readily transforms into the β-phase when mechanically deformed.[10] The δ-phase is a polar version of the α-phase, it is produced by subjecting an α-phase PVDF film to an electric field strong enough to polarize it.[10,11]

An increasing presence of polar crystallites will increase the maximum polarization and thus the piezoelectric constant d_{33} of PVDF.[12–14] Consequently, crystal formation has been well researched, especially in PVDF films. By mechanical deformation (stretching), β-phase can be formed from films predominantly consisting of α-phase PVDF. The degree of transformation from α to β increases with increasing draw ratio and draw rate, and drawing should take place at a temperature of 80°C–90°C.[12,14–16] At this stage, the local dipole moments of the β-phase crystallites will be randomly oriented in the PVDF structure. To render the whole structure polar, it is subjected to a high electric field which will induce a reorientation of the dipoles along the field direction (this process is known as poling). For this purpose, as well as for recording the piezoelectrically generated charge, electrodes must be added to two opposing surfaces of the material. In commercial PVDF films, the film surfaces are metalized and connected to metal wires. A large overlapping area of the electrodes will increase the piezoelectric output, so in fibers the electrodes should preferably be placed concentrically along the length of the fiber—as in a coaxial cable.

Correspondence to: B. Hagström (bengt.hagstrom@swerea.se).

Contract grant sponsors: Swedish Foundation for Strategic Research (SSF).

To date, research of piezoelectric PVDF in fiber form has mainly focused on fibers with diameters in the nanometer range produced by electrospinning, as this process has been shown to introduce β-phase crystallinity[17–19] as well as electrical polarization.[20,21] In one example, Wang et al.[21] showed that a fibrous sheet of PVDF nanofibers can be used as a sensor by adding electrodes on the top and bottom, similar to a film sensor. The sensor showed a sensitivity of 11–42 mV N^{-1}, depending on the degree of β-phase crystallinity in the samples. Chang et al.[19] used near-field electrospinning to manufacture piezoelectric nanogenerators by spinning PVDF nanofibers directly onto a substrate with electrodes. By stretching and releasing the substrate, an output of 5–30 mV and 0.5–3 nA could be produced.

Melt spun piezoelectric PVDF fibers have been produced by Walter et al.,[22] who manufactured a composite sensor by immersing parallel PVDF monofilaments in an epoxy resin and adding electrodes on the top and bottom of the flat sensor. After poling, the sensor showed an output of 0.09–7.39 V depending on the direction and mode of deformation. Recently, Egusa et al.[23] presented a piezoelectric coaxial fiber, where poly(vinylidene fluoride-trifluoroethylene) (P(VDF-TrFE)) constituted the electroactive component and the integrated electrodes were made from carbon-loaded polycarbonate and indium. These fibers were drawn from a preform, a multilayer rod. The advantage of P(VDF-TrFE) compared with PVDF is its ability to crystallize directly into the polar β-phase. However, the price is significantly higher.

We have previously shown that drawing in the solid state introduces β-phase crystallinity in melt spun PVDF fibers,[24] that a melt spinning process equivalent to that used in the industry can introduce β-phase in PVDF when properly tuned, and further that bicomponent PVDF fibers of a core/sheath structure can be spun with a carbon black (CB)/polymer compound useful as an integrated inner electrode.[25] However, we also showed that the solid state drawing necessary to introduce β-phase caused a significant decrease in the conductivity of the inner electrode.

Adding CB to a polymer matrix is by now a common way to make it electrically conductive. At a certain critical concentration—the percolation threshold—the CB will form a percolating network and conductivity is achieved. This network will also introduce solid-like rheological properties detrimental for spinnability.[26] Previous work from our group[27] has shown that at a melt draw ratio (MDR) of 100 a CB/PE compound could be melt spun with filler concentrations up to 7 wt %, while higher concentrations caused spinline break. Also, an increasing MDR caused a decrease in electrical conductivity—presumably as a result of the destruction of the percolating network by separation and orientation of the conducting particles. Spinnability could be enhanced by placing the CB compound in the core and using a highly spinnable polymer as sheath.[28] This is attributed to the fact that the sheath material bears a major share of the spin line force. The spinnability improved with increasing volumetric sheath/core ratio and became poorer with a lower viscosity sheath material.

The problem of a decreasing conductivity due to drawing can be remedied by heat treatment—by reheating a CB/polymer composite above its melting point, the electrical conductivity can be restored or at least improved. This has been explained by diffusion of the filler in the polymer resulting in increasing agglomeration of CB particles and diminishing separation distances between CB domains, resulting in a restored conductive network.[29,30] In addition to the restoration of the conductive network, the heat treatment causes a thermal expansion of the core. This is an important effect in bicomponent fibers as it will enhance the physical contact to the outer connections (silver paint) at the fiber ends thus significantly reducing the contact resistance.[28] In the case of piezoelectric PVDF fibers, the heat treatment temperature must be kept well below the Curie transition temperature, 170°C,[31] of PVDF.

In this article, bicomponent fibers with an enhanced electrical conductivity in the core material are produced and characterized with respect to their morphological, rheological, electrical, thermal, and mechanical properties. A sensor is manufactured by adding a common outer electrode to a number of fibers, and its piezoelectric properties are characterized.

EXPERIMENTAL SECTION—SAMPLE PREPARATION

Materials

A homopolymer PVDF was used as sheath material in the bicomponent fibers. The PVDF was Solef 1006, purchased from Solvay Solexis (Milan, Italy). According to the supplier, its melting point is 175°C, melt flow index (MFI) is 40 g/10 min at 230°C (for 2.16 g), and its density is 1780 kg m^{-3}. The electrodes (core and outer) consisted of electrically conductive compounds for which two matrix polymers, supplied by Dow (Midland, MI), were evaluated: (i) an ethylene-octene copolymer (CoPE) elastomer ENGAGE 8401; MFI = 30 g/10 min at 190°C for 2.16 g, density = 885 kg m^{-3} and melting point 80°C and (ii) a high density polyethylene (HDPE) ASPUN 6835A; MFI = 17 g/10 min at 190°C for 2.16 g, density = 950 kg m^{-3} and melting point 129°C. All data

presented here were given by the supplier. The polymer densities at 230°C—our processing temperature—are 1439 kg m^{-3} (PVDF) and 733 kg m^{-3} (PE).[32]

CB was supplied by AkzoNobel (Amersfoort, the Netherlands) under the commercial name Ketjenblack EC-600JD. The following properties were given by the supplier; electrical conductivity: 10–100 S cm^{-1}, aggregate size: 30–100 nm, and apparent bulk density: 100–120 kg m^{-3}. All materials were used as received.

Compounding

For conductivity measurements, compounding was done in a Brabender (Duisburg, Germany) AEV 651 kneader at 180°C. The matrix polymer was processed at 50 rpm for 3 min before adding CB. The blend was compounded at 100 rpm for 7 min. Compounds of both CoPE and HDPE were produced using 4, 6, 8, 10, and 12 wt % CB. The compounds were ground to granules in a Rapid (Bredaryd, Sweden) granulator.

For bicomponent melt spinning, larger amounts were required and compounded using a Coperion (Stuttgart, Germany) ZSK 26 K 10,6 twin screw extruder. The barrel temperature profile was set to 155°C, 195°C, and 205°C starting from the hopper inlet. Screw speed was 200 rpm. The extrudate was cooled on a conveyor belt at room temperature and ground to granules. The compounds produced for spinning were HDPE with 10 wt % CB and CoPE with 10 wt % CB. The CoPE+CB compound also constituted the outer electrode.

Sample preparation for initial conductivity measurements

The first samples for conductivity measurements were manufactured by extruding strands $\sim$ 1 mm diameter from a capillary rheometer (CEAST RHEOSCOPE 1000, Pianezza, Italy) using a die of 1 mm diameter and a length of 20 mm. The temperature was set to 180°C. Conductivity was also measured on a selection of bicomponent fibers, before and after heat treatment. Heat treatment was done for 10 min in an oven set to a temperature of 90°C for CoPE composite fibers and 140°C for HDPE composite fibers. The samples were cooled to room temperature before measurement.

Fiber spinning

Bicomponent fiber spinning was performed using a melt spinning line from Extrusion Systems Limited (ESL, Leeds, England) equipped with two single screw extruders, one for the core material, and one for the sheath material, see Figure 1. Their temperature settings were identical: extruder zones 1, 2, and 3 were set to 190°C, 220°C, and 230°C. The temperature of the gear pumps and spinneret was set to 230°C. For PVDF/CoPE+CB yarns, the spinneret used had 48 holes with a diameter of 0.6 mm and a land length of 1.2 mm. For PVDF/HDPE+CB yarns, the spinneret used had 24 holes with a diameter of 0.6 mm and a land length of 1.2 mm. The relative rate of metering of polymer to the spinneret controls the relative amounts of core and sheath material in the fiber.

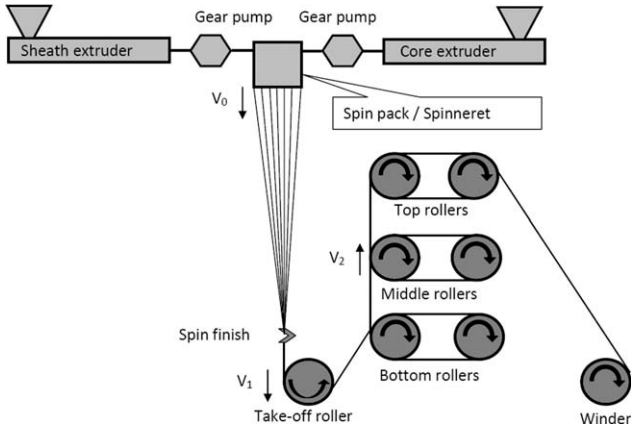

Figure 1 Schematic of the bicomponent fiber spinning machine.

Fibers were spun at different combinations of MDR and solid state draw ratio (SSDR) to find the maximum attainable SSDR before frequent spin line breakage occurred, see Table I. The diameter of the produced fibers is controlled by the draw ratio through the entire system. This draw ratio and the volume ratio were kept constant to produce fibers with comparable geometries.

Preparation of force sensor

A simple force sensor was manufactured by placing 10 yarns (240 fibers) of PVDF/HDPE+CB-4 in parallel between two thin conductive sheets consisting of a CoPE+CB compound with 10% CB. Here, the matrix polymer CoPE was selected for its low processing temperature. A thin copper wire was also sandwiched between the foils, and this system was compression molded between two object glasses in a heated press at 120°C. Thus, the molten sheets form the outer electrode in the form of a conductive matrix surrounding the fibers. The final thickness of the sensor was 0.48 mm. The inner electrodes were contacted by immersing the protruding fiber ends in conductive silver paint, which was expected to interconnect all the fibers' cores. The force sensor can be described as a number of piezoelectric coaxial fibers

TABLE I
Fiber Production Parameters, where MDR = V_1/V_0 and SSDR = V_2/V_1 (see Fig. 1)

Yarn	MDR	SSDR	Flow rate (cm^3 min^{-1}) Core	Flow rate (cm^3 min^{-1}) Sheath	V_0 (m min^{-1})	V_1 (m min^{-1})	V_2 (m min^{-1})	Roller temp (°C) Bottom	Roller temp (°C) Other
PVDF/CoPE+CB−1	137	1	7.2	28.56	2.64	342	370	80	RT
PVDF/CoPE+CB−2	68	2	7.2	28.56	2.64	169	361	80	RT
PVDF/CoPE+CB−3	45	3	7.2	28.56	2.64	113	369	80	RT
PVDF/CoPE+CB−4.5	30	4.5	7.2	28.56	2.64	73	361	80	RT
PVDF/HDPE+CB−4	23	4	7.2	28.56	5.27	116	489	90	RT
PVDF/HDPE+CB−4.75	20	4.75	7.2	28.56	5.27	98	489	90	RT

connected in parallel. The position of the electrodes will cause poling as well as piezoelectric charge to occur in the fiber's radial direction.

Poling

Poling of the sensor was done in an oven set to 100°C. A high voltage power supply ES50P-10W from Gamma High Voltage Research (Ormond Beach, FL) was connected to the sensor's electrodes, and the voltage was set to 1 kV. This corresponds to a field strength of 56 MV m^{-1} in the fiber sheath, which is sufficient to electrically polarize PVDF at this temperature.[33] The sample was cooled to room temperature before the voltage was removed.

EXPERIMENTAL SECTION—CHARACTERIZATION

Optical microscopy

Optical microscopy was done using a Nikon (Tokyo, Japan) SMZ1500 light microscope.

Tensile testing

The single filament titer values were examined using a Vibroscope from Lenzing (Lenzing, Austria). Tensile testing of single fibers was conducted on a Lenzing Vibrodyn. The distance between the clamps was 20 mm, and the test speed was 20 mm min^{-1}. A preload in the form of a small weight (200 mg) was attached to the filaments lower end. The results given are average values from 10 samples tested.

X-ray diffraction

For X-ray diffraction, a Bruker AXS (Madison, WI) D8 Advanced Theta X-ray powder diffractometer with monochromator was used. The radiation source was Cr Kα with a wavelength of 2.28970 Å. An increment step of 0.1° and a rate of 1 step per 10 s were used. The yarns were arranged in parallel to cover the surface of a flat sample holder, and attached by means of a double-sided adhesive tape. The sample holder rotated at 30 rpm throughout the measurement.

Thermal properties

Differential scanning calorimetry (DSC) analyses were performed using a TA Instruments (New Castle, DE) DSC Q2000. The specimen was placed in an aluminum vessel, which was crimped closed. Scans were performed at a heating/cooling rate of 10°C min^{-1}. Each sample was heated to well above its melting point and subsequently cooled and heated again. The results were analyzed using TA Instruments software Universal Analysis 2000. The reported data are average values from three samples, from the cooling and second heating cycles.

Viscosity

The viscosity as a function of shear rate was characterized on a Göttfert (Buchen, Germany) Rheograph 2002 capillary viscometer. The capillary had a flat entrance region, a length of 20 mm and a diameter of 1 mm. The pressure was measured just above the capillary, using a transducer with a pressure range of 0–500 bar. The heated cylinder had a diameter of 12 mm, the test temperature was set to 230°C, and the piston speed was stepwise incremented as follows: 0.265–0.53–1.061–2.12–4.25–8.5 mm min^{-1}. At least three measurements were performed on each material, and all experimental data were subjected to the Rabinowitsch correction.[34]

Electrical conductivity

A two-point setup was used for DC conductivity measurements. On the extruded strands, crocodile clips were connected to each end, a voltage was applied, and the current was measured. For characterization of the bicomponent yarns, the yarn ends were coated with silver paint and contacted with crocodile clips. The calculated electrical conductivity refers to the core material only. The amount of core material in the bicomponent fibers was calculated

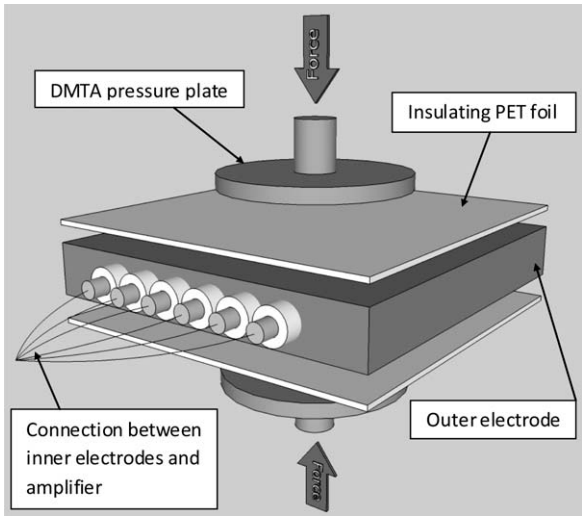

Figure 2 Schematic of the force sensor and its position in the DMTA equipment.

from the extrusion parameters (volumetric flow rate of sheath and core material) and the density of sheath and core material at the processing temperature. The electrical conductivity σ_v is calculated as:

$$\sigma_v = I\rho l^2/(Um) \quad (1)$$

where I is the measured current, ρ is the density, l is the length of fiber between the clips, U is the measured voltage, and m is the mass of fiber between the clips. The power source used was D400-007D from Oltronix (Em Leek, Holland). The voltage and current were measured using Fluke 111 True RMS multimeters from Fluke (Solna, Sweden). All measurements were done in a laboratory with constant air humidity at 30%. Conductivity was measured on three samples, and average values were calculated.

RC-measurements of the sensor

The resistance and capacitance of the sensor was measured using a HP Precision LCR meter 4284A from Agilent technologies (Santa Clara, CA). In the measurement, the capacitance and resistance were pictured as being parallel configured. The measurements were performed between 20 Hz and 30 kHz.

Electromechanical characterization

For piezoelectric characterization, the sensor was subjected to a dynamic compression strain perpendicular to the fiber axis (see Fig. 2) in a Rheometrics DMTA-equipment (RSA II), with a plate-to-plate setup. Small pieces of a thin (thickness ≈ 0.04 mm) polyethyleneterphtalate (PET) film were placed between the sensor and the metallic plates to ensure electrical insulation. The bias force was 0.75 N. In the oscillating mode, a sinusoidal strain with a maximum value of 2% was applied, and the output voltage was measured. Next, a pulsed strain of 3% was applied, and the step response was measured.

The sensor electrodes were connected to an AC coupled high impedance amplifier, Model 1201 from DL Instruments (Ithaca, NY), with gain = 10 and input impedance = 100 MΩ. The output signal from the amplifier was sampled using a data acquisition device, NI DAQPad-6016, from National Instruments (Austin, TX) connected to a computer running a LabVIEW Software, which controlled the measurement. The piezoelectric signals were slightly filtrated to reduce high frequency noise. In addition, two analog signals from the RSA II proportional to the strain and force were continuously sampled.

RESULTS AND DISCUSSION

Thermal properties and viscosity

In Figures 3–5, representative DSC thermograms from cooling and second heating of the bicomponent fibers and the respective polymers are shown. Apparently, the addition of CB has a small effect on the transition temperatures. The thermograms confirm that solid state drawing of the PVDF/HDPE+CB fibers was performed under the melting point of the core material, while the PVDF/CoPE+CB fibers were drawn close to the melting point of the core material.

Figure 6 shows results from the viscosity measurements. As expected, the addition of CB causes an increase in the viscosity of CoPE and HDPE. The shear rate at the wall in the spinneret holes was about 600 and 1200 s^{-1} for the 48 and 24 hole spinneret, respectively. In this range of shear rates, the core material (CoPE+CB or HDPE+CB) has a similar

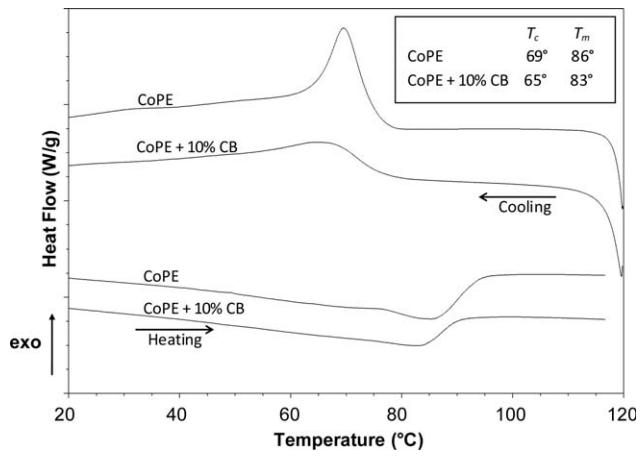

Figure 3 DSC thermograms for CoPE with and without filler.

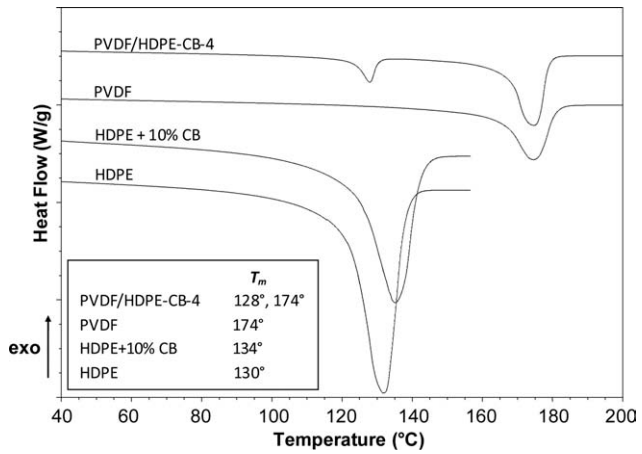

Figure 4 Melting endotherms for bicomponent fiber PVDF/HDPE-CB-4 and its components.

or somewhat higher viscosity compared to the sheath material (PVDF). This is normally recommended for a stable coaxial coextrusion flow.

Electrical conductivity of the inner electrode

The electrical conductivity as a function of CB content was measured on extruded strands from the two composites. The data were fitted to a line by means of least squares regression, see Figure 7. The percolation threshold may be calculated from the conductivity relationship[35]:

$$\sigma = k(w - w_c)^{\beta} \tag{2}$$

where k is a constant related to the conductivity of the filler, w is the weight fraction of filler, w_c is the weight fraction at the percolation threshold, and β is the critical exponent.

By resolving the unknown variables from the graph in Figure 7, the percolation thresholds of both

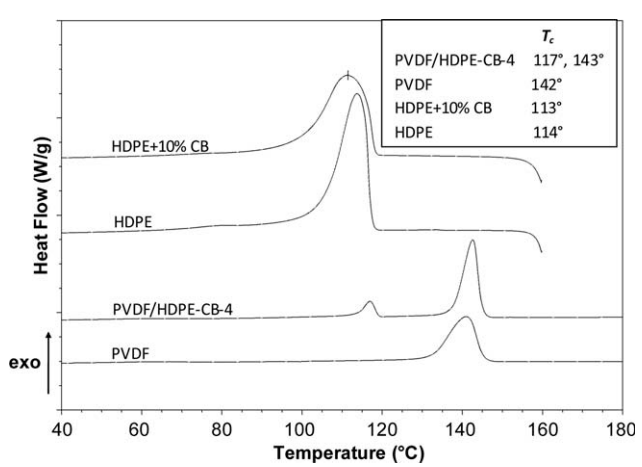

Figure 5 Crystallization exotherms for bicomponent fiber PVDF/HDPE-CB-4 and its components

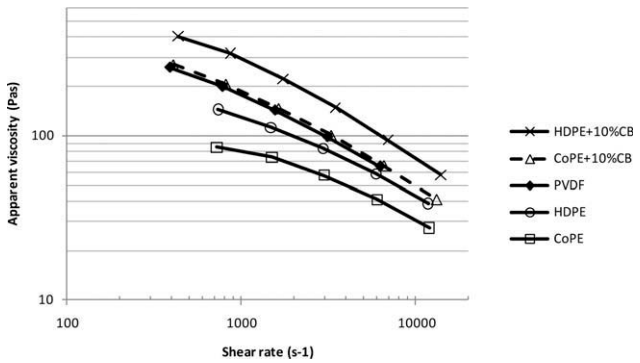

Figure 6 Representative viscosity curves for the polymers and their blends with CB.

composites were calculated to be ~ 4 wt % CB. As can be seen from the standard deviation values given in Figure 7, the conductivities measured at low CB loadings are rather uncertain also rendering the exact percolation threshold uncertain. Although the percolation curves are similar, the CB/HDPE compound shows a higher conductivity at high concentrations of CB. This is possibly due to the higher degree of crystallinity in HDPE, promoting a two-phase system which is advantageous for electrical conductivity.[29]

Figure 8 shows the electrical conductivity of the core material in the bicomponent yarns PVDF/CoPE+CB-4.5 and PVDF/HDPE+CB-4, both using 10 wt % CB. As expected, the electrical conductivity is significantly decreased by the spinning process. For the HDPE/CB composite, the conductivity decreases from 0.22 (see Fig. 7) to 0.04 S cm^{-1}, for CoPE/CB the corresponding values are 0.11 and 0.008 S cm^{-1}.

Figure 8 also shows that heat treatment of our bicomponent yarns had varying effects on the conductivity. Although the core conductivity of the PVDF/HDPE+CB increases, the PVDF/CoPE+CB

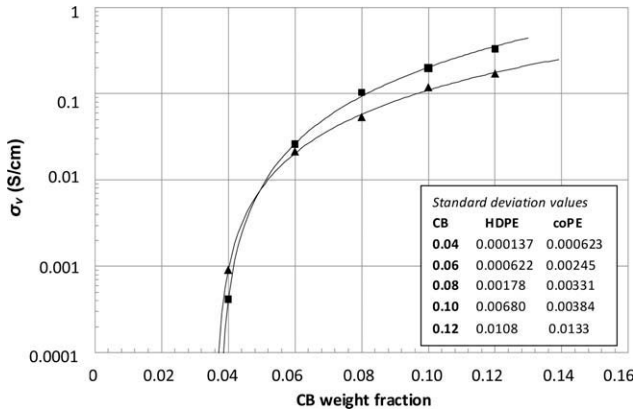

Figure 7 Electrical conductivity as a function of CB weight fraction, for extruded strands of HDPE based composites (■) and CoPE based composites (▲). Lines indicate the calculated percolation curve.

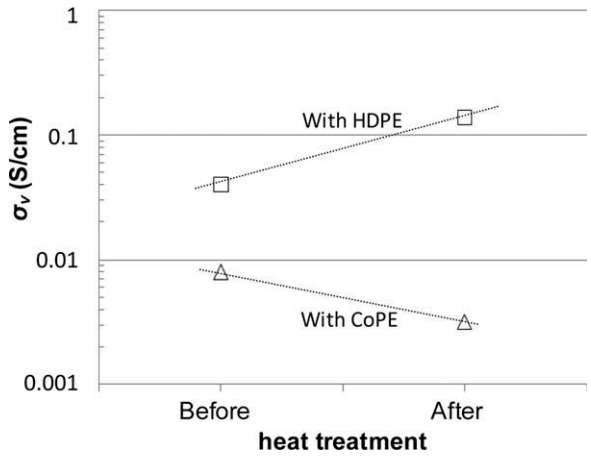

Figure 8 Electrical conductivity of the core in bicomponent fibers PVDF/CoPE+CB-4.5 (Δ) and PVDF/HDPE+CB-4 (□), both with 10 wt % CB, before and after heat treatment.

yarns show a significant decrease in conductivity after heat treatment. This is probably related to the lower T_m of CoPE; solid state drawing in our spinning process was done at 80°C, where CoPE is likely to still be mainly in its molten state. It may be suggested that when CoPE is melted a second time, during heat treatment, the CB agglomerates have reached a size where the distances between them are increasing thus again lowering the conductivity.

Morphology

Figures 9 and 10 show X-ray diffractograms for the bicomponent fibers in varying stages of solid state drawing. The bottom curves show diffractograms for the respective filler materials. From the PVDF/HDPE+CB fiber before drawing, three peaks typical for PVDF α-phase (see Table II) can be seen. There is also one peak at 2Θ = 32.5°, which is apparently related to the core material HDPE+CB. The curves for fibers at the higher SSDRs are similar and show one dominant peak around 31°, typical for the β-phase. Thus, the prerequisite of polar crystal phase is fulfilled by these fibers.

Piezoelectric properties

The fibers denoted PVDF/HDPE+CB-4, shown in Figure 11, were selected for piezoelectric characterization for two reasons; the HDPE compound showed a higher electrical conductivity than the CoPE compound, and at SSDR = 4, the spinning process was stable while higher draw ratios caused frequent spinline breakage. The fiber diameter was ~ 60 μm, with a core diameter of 24 μm, and a sheath thickness of 18 μm. Titer was 40 dTex/fiber. The tenacity of PVDF/HDPE+CB-4 was 24.8 cN tex^{-1} (±1.7), elongation at break was 60.7% (±10.4), and the elastic modulus was 181 cN tex^{-1} (±12). The mechanical properties of the fibers were proven to be well suited for downstream textile conversion methods like weaving and knitting. We have successfully used them as weft and produced a woven textile in an industrial type projectile weaving machine.

A sensor, shown in Figures 12 and 13, was manufactured as described in the experimental section. Its resistance and capacitance are shown as a function of frequency in Figure 14. Figure 15 shows the resulting force and piezoelectric signal generated by the sensor when compressed at two different frequencies, 10 and 1 Hz. A similar, but unpoled, sensor was also tested but did not produce any piezoelectric response, as shown in Figure 16. Clearly, the poling process successfully introduced a radial alignment of the dipoles/crystallites.

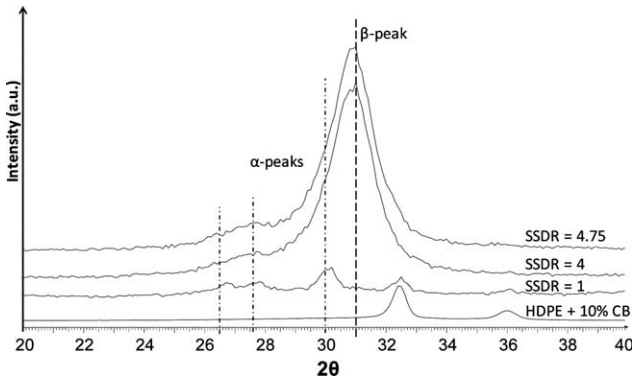

Figure 9 X-ray diffractograms of PVDF/HDPE+CB bicomponent fibers spun with SSDR = 4 and 4.75 (sheath/core ratio 12/3). The undrawn filaments (SSDR = 1) had sheath/core ratio 10/6. The bottom curve shows the result from a pressed film of the CB/HDPE compound. The curves have been shifted along the intensity axis for better clarity.

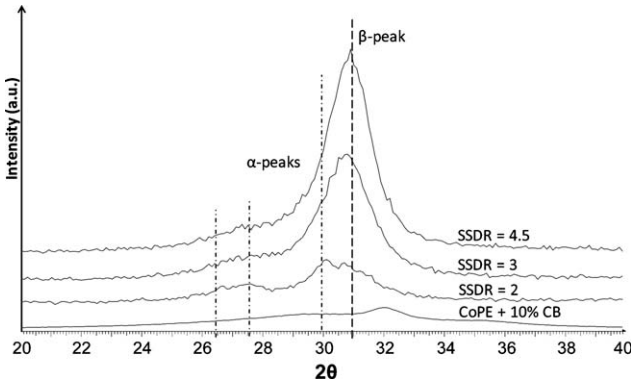

Figure 10 X-ray diffractograms of PVDF/CoPE+CB bicomponent fibers spun with SSDR = 2, 3, and 4.5 (sheath/core ratio 12/3). The bottom curve shows the result from a pressed film of the CB/CoPE compound. The curves where shifted along the intensity axis for better clarity.

TABLE II
Inter-Planar Distances and Corresponding 2Θ Angles for Maximum Intensity Peaks in XRD, According to the Literature

α-phase[4–6,36–38]			β-phase[4–8,36,37]		
hkl	*d* (Å)	2Θ	hkl	*d* (Å)	2Θ
110	4.39 − 4.45	29.8° − 30.2°	110/200	4.23 − 4.33	30.7° − 31.4°
200	4.79 − 4.82	27.5° − 27.7°			
010	4.92 − 5.10	26.0° − 26.9°			

As can be seen in Figure 15, the applied force and the piezoelectric response are in phase at 10 Hz but in the case of 1 Hz there is a phase shift of about 36°. Also a small attenuation (∼ 4%) of the signal amplitude can be seen in the 1 Hz measurement compared with the one at 10 Hz. In Figure 17, the strain signal and output force for the above measurement are shown. In this case, the signals are in phase at 1 Hz while at 10 Hz there is a small phase shift, probably due to the viscoelastic properties of the electrode material. This implies that the phase shift at 1 Hz, seen in Figure 15, is related to the electrical properties of the sensor rather than its mechanical properties.

Electrically, the sensor can be seen as a high pass filter (HP-filter); a circuit that consists of a resistance in parallel with a capacitor and a voltage source[39] and therefore passes signals unaffected at high frequencies but attenuates signals below the filter's cut off frequency (f_c). Both the phase shift and the attenuation effect seen in Figure 15 are characteristic for a HP-filter. The f_c will be determined not only by the sensor specific resistance and capacitance but also by the input impedance of the measurement equipment connected to the sensor. It can be calculated from eq. (3):

$$f_c = 1/(2\pi RC) = 1/(2\pi\tau) \quad (3)$$

where R is the resistance of the system (sensor and measurement equipment), C is the capacitance of the system, and τ is the filter time constant; the time it takes for the signal to reach $1 - 1/e \approx 63\%$ of its initial value V_0. C in our system can be assumed to be equivalent to the sensor's capacitance, while R is equivalent to the resistance of the measurement system (at 1 Hz, $R_{sensor} \gg R_{meas}$). So in our system, $R =$ 100 MΩ, $C \approx 2.1$ nF (estimated from Fig. 14) thus $f_c \approx 0.75$ Hz. Figure 18 shows the piezoelectric response amplitude over the applied force amplitude of the compression plotted as a function of frequency of the applied force. Here, the HP-filter characteristics are clearly seen, and the maximum value (19.5 mV N^{-1}) of the piezoelectric response is reached at around 10 Hz.

Figure 19 shows the results from a step response measurement. When the compression force pulse is applied, there is a fast change in the sensor output voltage, followed by a slow decrease of the generated voltage. The same behavior occurs when the compression force is released but now the generated piezoelectric signal has the opposite sign. The sign convention is correlated to which sensor electrode (core or outer) is connected to the positive amplifier input. The applied pulse amplitude of 1.9 N resulted in a measured piezoelectric response factor ∼ 17 mV N^{-1}. The result in Figure 19 illustrates an important property of a piezoelectric sensor; it is only sensitive to dynamic forces and not to static ones, and its response depends on the characteristic relaxation time. The shape of the discharging curve is also useful to confirm the f_c; for our sensor, $\tau = 0.27$ s which

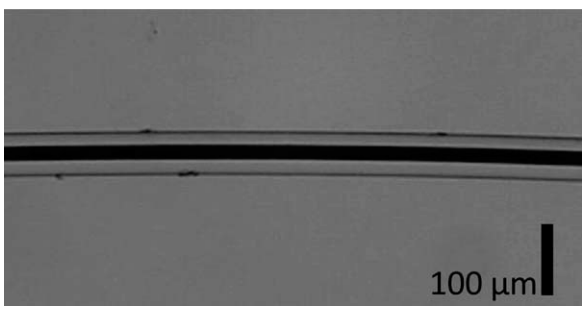

Figure 11 Optical micrograph of a piezoelectric bicomponent fiber. The core (black) consists of HDPE with 10 wt % CB. The sheath (transparent) is PVDF.

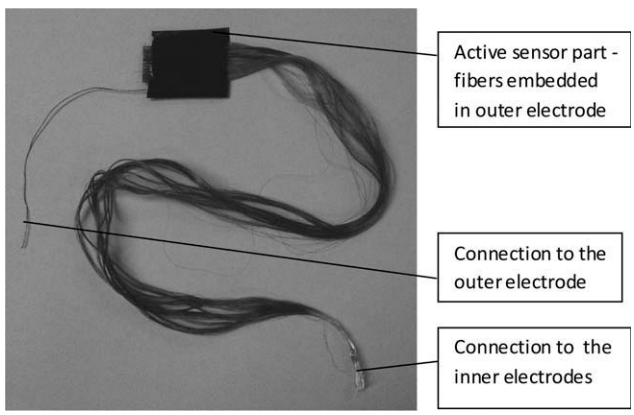

Figure 12 Simple force sensor made from bicomponent fibers.

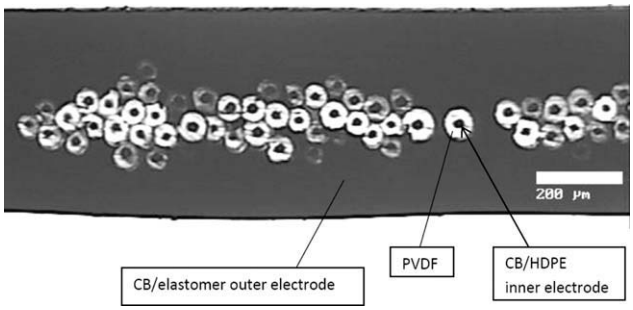

Figure 13 Optical micrograph of a cross-section of the force sensor. Scale bar is 200 μm.

corresponds to an $f_c \sim 0.60$ Hz. This is in accordance with the frequency response shown in Figure 18.

To estimate the piezoelectric charge constant d for the piezo-fiber sensor, according to eq. (4)[39] below, we effectively regard it as a piezoelectric film (one single piezo film sensor instead of many piezo fibers in parallel). We must take into account that (i) the outer electrode covers two sides of the sensor [which adds the factors of 2 in eq. (4)], and (ii) the voltage attenuation due to the fact that only a part of the sensor area is subjected to a force (this gives the A/A_L term in the numerator). So

$$d = \frac{Q}{2A\left(F/A_L\right)} = \frac{C\left(A/A_L\right)V}{2A\left(F/A_L\right)} = \frac{CV}{2F} \qquad (4)$$

where Q is the piezoelectrically generated charge, A is the electrode area, F is the applied force, A_L is the electrode area actually subjected to a load, and V is the piezoelectrically generated output voltage above f_c (where the response is more or less saturated). For

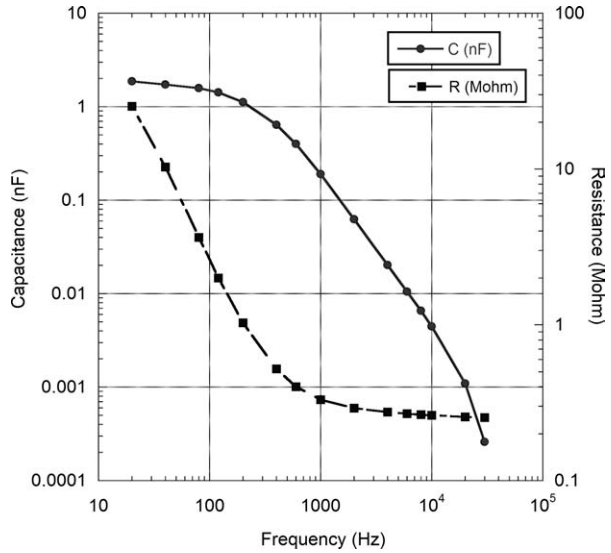

Figure 14 Capacitance and resistance of the sensor, as a function of frequency.

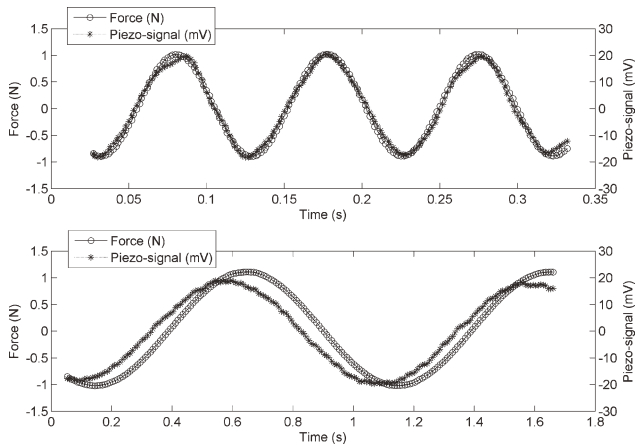

Figure 15 Example of the resulting force and voltage output as a function of time during an oscillating compression at 10 Hz (upper figure) and 1 Hz (lower figure).

our sensor, $V = 19.5$ mV N^{-1} and $C = 2.1$ nF (the measured capacitance at a frequency just above f_c). The thus obtained d values are in the order of 20 pC N^{-1}, which is comparable with the piezoelectric charge constants of commercial PVDF piezoelectric films.[39]

The setup used here does not allow us to calculate the piezoelectric charge constant of single fibers for several reasons: although the output from our fibers is measured in the radial direction (equivalent to the thickness direction in films), they are not subjected to forces solely in this direction. Furthermore, as can be seen in Figure 13, the fibers are not symmetrically distributed within the conductive matrix, and not all fibers are in perfect contact with the outer electrode. An improved design of the outer electrode would probably result in a higher piezoelectric response.

In our force sensor, the compression of the fibers is not all in the same directions as the radial polarization directions of the piezo-fibers and the compression in one direction of the fiber is accompanied by an expansion of the fiber in the orthogonal direction. Thus, the piezoelectric response of the sensor is

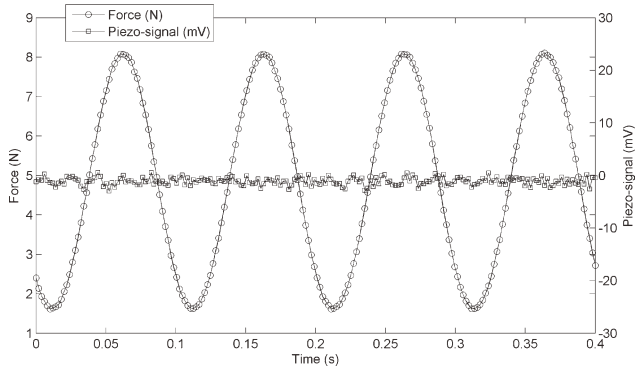

Figure 16 Measured force and output voltage from the sensor before poling.

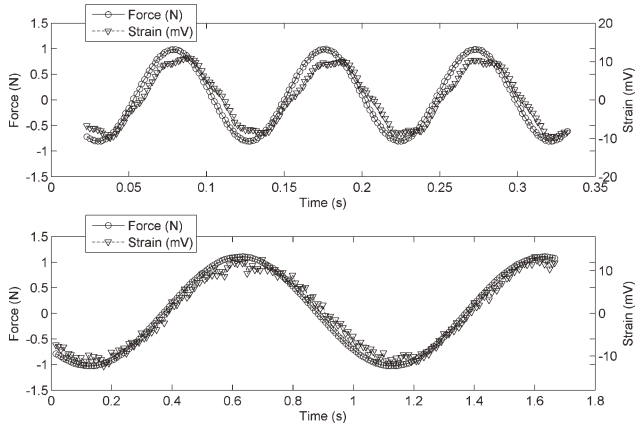

Figure 17 Example of the strain (actually strain gauge output signal) and resulting force signals as a function of time, during an oscillating compression at 10 Hz (upper figure) and 1 Hz (lower figure).

in some part reduced. The mode of deformation plays an important role for the resulting output voltage. It can be noted that the piezoelectric response in axial elongation is quite strong. Preliminary results indicate an output of several tens of volts at 5 Hz and 1% strain. The characterization of our fibers in axial tension is the subject of a coming paper.

CONCLUSIONS

The melt spinning of a novel piezoelectric bicomponent polymer fiber, with PVDF as the electroactive component, has been demonstrated. An electrically conductive compound of CB and HDPE was used as core material, working as an inner electrode. A force sensor, consisting of a number of fibers embedded in a soft CB/CoPE elastomer matrix, was manufactured for piezoelectric characterization. The fibers showed a clear piezoelectric effect comparable with that of commercial piezoelectric polymer films, with a voltage output of up to 20 mV N^{-1} under lateral compression, and several tens of volts in axial tension. The sensor manufacturing technology presented here can very well be developed toward producing single yarn or single fiber sensors.

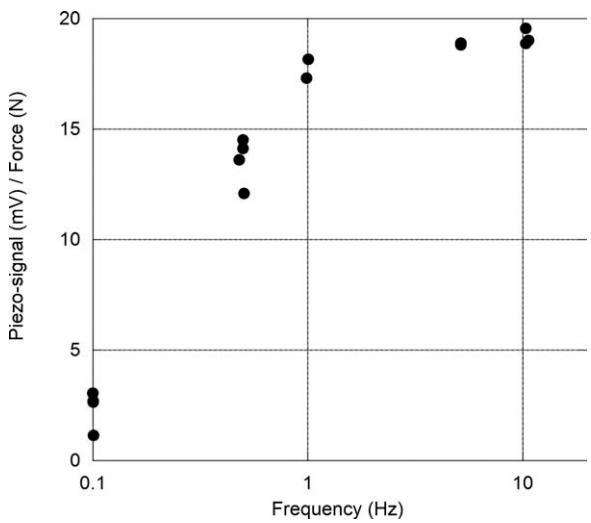

Figure 18 Piezoelectric response of the sensor as a function of compression frequency.

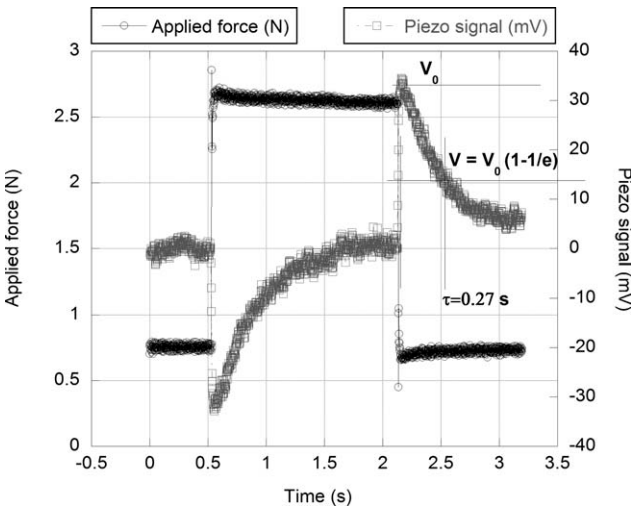

Figure 19 Results from a step response measurement for the piezo-fiber sensor. The generated force and piezoelectric signal are plotted as a function of time during a pulse shaped compression.

References

1. Kawai, H. Jpn J Appl Phys 1969, 8, 975.
2. Fukada, E.; Takashita, S. Jpn J Appl Phys 1969, 8, 960.
3. Lenk, A.; Ballas, R. G.; Werthschützky, R.; Pfeifer, G. Electromechanical Systems in Microtechnology and Mechatronics, Part 3; Springer-Verlag: Heidelberg, 2011.
4. Lando, J. B.; Doll, W. W. J Macromol Sci Phys 1968, B2, 205.
5. Matsushige, K.; Nagata, K.; Imada, S.; Takemura, T. Polymer 1980, 21, 1391.
6. Das Gupta, D. K.; Doughty, K. Appl Phys Lett 1977, 31, 585.
7. Hasegawa, R.; Takahashi, Y.; Chatani, Y.; Tadokoro, H. Polym J 1972, 3, 600.
8. Teulings, R. P.; Dumbleton, J. H.; Miller, R. L. Polym Lett 1968, 6, 441.
9. Samon, J. M.; Schultz, J. M.; Hsiao, B. S.; Seifert, S.; Stribeck, N.; Gurke, I.; Collins, G.; Saw, C. Macromolecules 1999, 32, 8121.
10. Weinhold, S.; Litt, M. H.; Lando, J. B. Macromolecules 1980, 13, 1178.
11. Bachmann, M.; Gordon, W. L.; Weinhold, S.; Lando, J. B. J Appl Phys 1980, 51, 5095.
12. Mohammadi, B.; Yousefi, A. A.; Bellah, S. M. Polym Test 2007, 26, 42.
13. Broadhurst, M. G.; Davis, G. T.; McKinney, J. E.; Collins, R. E. J Appl Phys 1978, 49, 4992.
14. Gomes, J.; Serrado Nunes, J.; Sencadas, V.; Lanceros-Méndez, S. Smart Mater Struct 2010, 19, 1.
15. Sajkiewicz, P.; Wasiak, A.; Goclowski, Z. Eur Polym J 1999, 35, 423.

16. Sobhani, H.; Razavi-Nouri, M.; Yousefi, A. A. J Appl Polym Sci 2007, 104, 89.
17. Wu, A. Y.; Kotaki, M.; Liu, Y.; Lu, X. Polymer 2007, 48, 512.
18. Huang, S.; Yee, W. A.; Tjiu, W. C.; Liu, Y.; Kotaki, M.; Boey, Y. C. F.; Ma, J.; Liu, T.; Lu, X. Langmuir 2008, 24, 13621.
19. Chang, C.; Tran, V. H.; Wang, J.; Fuh, Y.-K.; Lin, L. Nano Lett 2010, 10, 726.
20. Andrew, J. S.; Clarke, D. R. Langmuir 2008, 24, 670.
21. Wang, Y. R.; Zheng, J. M.; Ren, G. Y.; Zhang, P. H.; Xu, C. Smart Mater Struct 2011, 20, 1.
22. Walter, S.; Steinmann, W.; Schütte, J.; Seide, G.; Gries, T.; Roth, G.; Wierach, P.; Sinapius, M. Mater Technol 2011, 26, 140.
23. Egusa, S.; Wang, Z.; Chocat, N.; Ruff, Z. M.; Stolyarov, A. M.; Shemuly, D.; Sorin, F. Nat Mater 2010, 9, 643.
24. Lund, A.; Hagström, B. J Appl Polym Sci 2010, 116, 2685.
25. Lund, A.; Hagström, B. J Appl Polym Sci 2011, 120, 1080.
26. White, J. L.; Tanaka, H. J Appl Polym Sci 1981, 26, 579.
27. Stråât, M.; Toll, S.; Boldizar, A.; Rigdahl, M.; Hagström, B. J Appl Polym Sci 2011, 119, 3264.
28. Stråât, M.; Rigdahl, M.; Hagström, B. J Appl Polym Sci 2012, 123, 936.
29. Foulger, S. H. J Appl Polym Sci 1999, 72, 1573.
30. Alig, I.; Skipa, T.; Lellinger, D.; Pötschke, P. Polymer 2008, 49, 3524.
31. Teyssedre, G.; Bernes, A.; Lacabanne, C. J Polym Sci Part B: Polym Phys 1995, 33, 879.
32. Zoller, P.; Walsh, D. J. Standard Pressure-Volume-Temperature Data for Polymers; Technomic Publishing AG: Basel, 1995.
33. Wang, T. T.; Herbert, J. M.; Glass, A. M., Eds. The Applications of Ferroelectric Polymers; Chapman and Hall: Glasgow, 1988.
34. Barnes, H. A.; Hutton, J. F.; Walters, K. An Introduction to Rheology; Elsevier: Amsterdam, 1989.
35. Stauffer, D. Introduction to Percolation Theory; Taylor & Francis: London, 1985.
36. Wang, Y.; Cakmak, M.; White, J. L. J Appl Polym Sci 1985, 30, 2615.
37. Zhang, H.; Ren, P.; Zhang, G.-F.; Xiao, C.-F. J Wuhan Univ Technol 2006, 21, 53.
38. Li, X.; Lu, X. J Appl Polym Sci 2007, 103, 935.
39. Piezo Film Sensors, Technical Manual; Measurement Specialties, Inc.: Hampton, 2008.